Scripta Materialia 168 (2019) 1–4

Contents lists available at ScienceDirect

Scripta Materialia

journal homepage: www.elsevier.com/locate/scriptamat

Atomic force microscopy study of nanoporous gold surface and electrochemical properties

Panpan Gao [a,b], Ping Qian [a,b], Lijie Qiao [a,c], Alex A. Volinsky [d], Yanjing Su [a,c,*]

[a] Beijing Advanced Innovation Center for Materials Genome Engineering, University of Science and Technology Beijing, Beijing 100083, China
[b] Department of Physics, University of Science and Technology Beijing, Beijing 100083, China
[c] Advanced Material and Technology Institute, University of Science and Technology Beijing, Beijing 100083, China
[d] Department of Mechanical Engineering, University of South Florida, Tampa, FL 33620, USA

ARTICLE INFO

Article history:
Received 23 February 2018
Received in revised form 20 December 2018
Accepted 6 January 2019
Available online xxxx

Keywords:
Nanoporous gold
Dealloying
Coarsening
Atomic force microscopy

ABSTRACT

The morphology, surface oxide and strain evolution of nanoporous (np) gold were investigated using atomic force microscopy (AFM). Topographic AFM images show typical np structure with a few nanometers ligament size. Current sensing AFM results revealed semiconductor properties of the surface oxide, which may consist of Ag_2O (p-type) and AgO (n-type). The surface oxide can effectively suppress the np structure coarsening. *In-situ* electrochemical AFM tests exhibit a refined macroscopic dimensional change of 40 nm within 0.35–0.7 V potential range. AFM can be used as an effective method to investigate the morphology and voltage-induced dimension changes in electrolyte.

Nanoporous (np) metals with bi-continuous open porosity have the potential to outperform existing materials in various technological applications, such as catalysts [1–3], plasmonics [4,5], electrochemical supercapacitors [6], actuators [7–11], sensors [12–16], and battery electrodes [17–19]. Nanoporous metals are fabricated by dealloying or electrochemical dealloying, in which the less noble components are selectively dissolved from a homogenous alloy, and the more noble components are left behind to form the three-dimensional metal skeleton. Nanoporous gold (npg) exhibits a typical sponge-like open cell foam structure formed by dealloying silver from the AgAu alloy. The resulting npg samples had 70–80% porosity and 3–50 nm ligament size, and maintained the original macroscopic shape of the alloy samples [20]. More recently, many efforts have been devoted to studying the chemically and electrochemically-induced strain in npg [7,16] which may be utilized in sensing and actuation applications. Furthermore, detailed characterization of structures and surface properties of np ligaments during dealloying process is an emerging fundamental research field.

In recent decades, many researchers have attempted to investigate dealloying process and the underlying physical mechanisms in np metals. The dealloying process can be regarded as a competition between selective dissolution, which roughens the surface and surface diffusion, which smoothens the surface [21]. The physical mechanisms of dealloying have been discussed according to the corrosion disordering/diffusion reordering model, the dynamic roughening transition model, and the kinetic Monte Carlo model [22]. The dealloying begins with the dissolution of a single silver atom on a flat alloy surface of closed pack (111) orientation, leaving a terrace vacancy behind. Then the adatoms diffuse and start to agglomerate into islands before the next layer is attacked. Thus, the pore forms due to the more noble atoms being chemically driven to aggregate into two-dimensional clusters by a phase separation process. Jin et al. [23] suggested that an oxide layer formed during dealloying and the npg samples exhibit extraordinarily small 1–2 nm structure of the material. Also, the samples revealed a large reversible elastic contraction during the anodic part of the cyclic potential scan, which is opposite to the clean surface samples.

Currently, the most popular method for controlling the morphology of np metals is by coarsening of ligaments and pores during thermal or acid post-treatments, where np specimens are either exposed to high temperature or kept in an acid environment after dealloying. According to the Kertis et al., the pore size of npg can be further affected by thermal annealing, and finally achieve over 10 μm size [24]. When considering npg annealing, one should be aware that it is important to thoroughly clean any electrolyte off the sample and start with a fully reduced surface because the bumpy and sharp features of the sample annealed without reduction have clearly inhibited coarsening and led to a more random, bumpy and finer scale material [24]. For npg, the coarsening of ligaments and pores is driven by the reduction of the surface free energy, which involves surface diffusion of gold atoms in order to form np structures with minimal surface energy [25]. Some strategies have been

* Corresponding author at: Beijing Advanced Innovation Center for Materials Genome Engineering, University of Science and Technology Beijing, Beijing 100083, China.
E-mail address: yjsu@ustb.edu.cn (Y. Su).

https://doi.org/10.1016/j.scriptamat.2019.03.044
1359-6462/

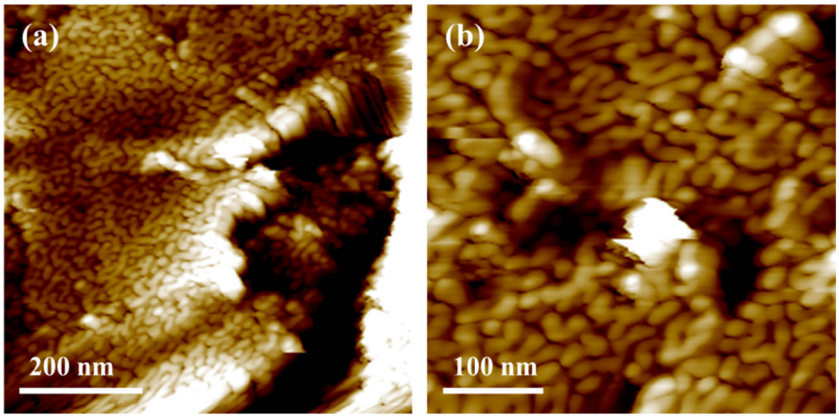

Fig. 1. AFM topography images of (a) the initial prepared NPG-1 sample and (b) reduced NPG-3 sample.

devised to reduce coarsening, such as adding noble alloying elements [26], controlling the dealloying conditions [27] and forming the surface oxide [23]. These studies point out the importance of surface oxide and its properties for the np structure formation and the coarsening process.

Atomic force microscopy (AFM) is a technique used to characterize the surface morphology and investigate the surface properties of many different materials with near atomic resolution. Current sensing AFM (CSAFM) is a technique to map the current between the conductive tip and the surface with nanometer spatial resolution [28]. CSAFM can acquire the electrical conductivity of the micro-area of the samples by measuring the current at a given applied voltage, along with obtaining local current-voltage (I-V) curves. The force between the tip and the sample surface can be adjusted. Thus, CSAFM is regarded as an effective tool to investigate the local surface semiconductor properties, so the oxide state and properties can be characterized. Electrochemical AFM (EC-AFM) in ambient conditions with potentiostatic control is used to monitor macroscopic dimensional response during potential sweeping in electrolyte. The electrochemical cell used in EC-AFM was made of Teflon. It consisted of Pt as the counter and reference electrodes, and the sample as the working electrode. The potential for the *in-situ* study was varied from 0.35 V to 0.7 V according to the cyclic voltammogram (CV). During potential sweeping, the AFM will record the height changes on the sample surface based on the interaction between the tip and the sample. Thus, the sample macroscopic dimension changes can be detected, recording the strain evolution during the potential change.

$Au_{25}Ag_{75}$ ingots were prepared by the arc-melting of the high purity (>99.99%) silver and gold wires in argon atmosphere. The ingots were homogenized at 850 °C for >100 h, cut into 1.2 × 1.2 × 2 mm^3 samples and then annealed at 600 °C for 4 h. The dealloying of the alloy samples was performed under potentiostatic control (AUTOLAB PGSTAT302N) in 1 M $HClO_4$ at ambient temperature. A silver wire and a pseudo Ag/AgCl reference electrode were used as the counter and reference electrodes in the dealloying process, respectively. The Ag/AgCl reference electrode potential is ~0.53 V more positive than the standard hydrogen electrode (SHE). Aqueous solution was prepared from guaranteed reagent grade $HClO_4$ (Sinopharm Chemical Reagent Co., Ltd.) and ultrapure water (18.2 MΩ). The morphology and the ligament size were characterized using scanning electron microscopy (SEM, FEI NOVA SEM430) of the cross-sectioned np sample surfaces. The residual Ag content was measured using energy dispersive spectroscopy (EDS, FEI NOVA SEM430) on the np samples cross-section surface. All measurements were carried out at room temperature.

The initial npg sample NPG-1 was prepared by dealloying at 0.7 V which took around 30 h. It is noted that the NPG-1 contains a high concentration of residual silver (~23 at.%) with a ligament size of 15 nm. The top surface morphology of NPG-1 obtained by the contact mode AFM is shown in Fig. 1a. Secondly, the NPG-2 sample was prepared by polarizing at a higher potential of 1.0 V to further dissolve Ag from NPG-1. The ligament size of NPG-2 is almost the same as the initial prepared NPG-1. The residual Ag content in NPG-2 is decreased to around 5 at.%. In the last step, the NPG-2 sample was treated at 0.7 V for surface desorption, so that the reduced sample NPG-3 can be obtained. Fig. 1b shows the AFM topography of the NPG-3 sample with a larger ligament size of 30–40 nm compared with the first two samples. This indicated that the surface adsorption of NPG-2 played a key role in suppressing the structure coarsening.

To further investigate the surface properties of the polarized npg sample NPG-2, the CSAFM measurements have been carried out using Agilent 5500 AFM (Agilent Technologies, USA) operated in the current sensing mode. The probes used were DPE14/AIBS conductive Pt-coated silicon tips with 5.7 N/m force constant. CSAFM uses contact AFM mode with a voltage bias applied to the tip, while scanning the sample surface, the surface topography can be obtained. Local I-V curves can be also obtained by placing the tip at a fixed position on the npg surface chosen randomly. Dozens of different positions were investigated on the scanned surface, and local I-V curves were obtained, as shown in Fig. 2, which presents three typical characteristics: linear, almost symmetric and asymmetric. There are some obvious differences between these positions. Generally, the I-V curves are expected to be linear for metals, since they are conductors. Clearly, there are also some positions showing different features in the I-V curves, which are nonlinear and asymmetric.

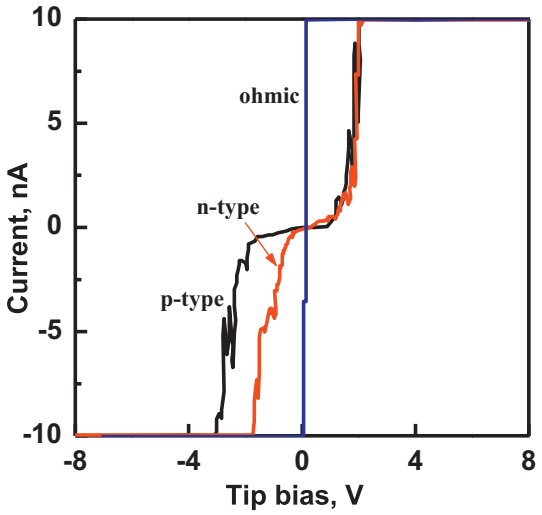

Fig. 2. Typical I-V curves obtained from CSAFM of the polarized NPG-2 sample.

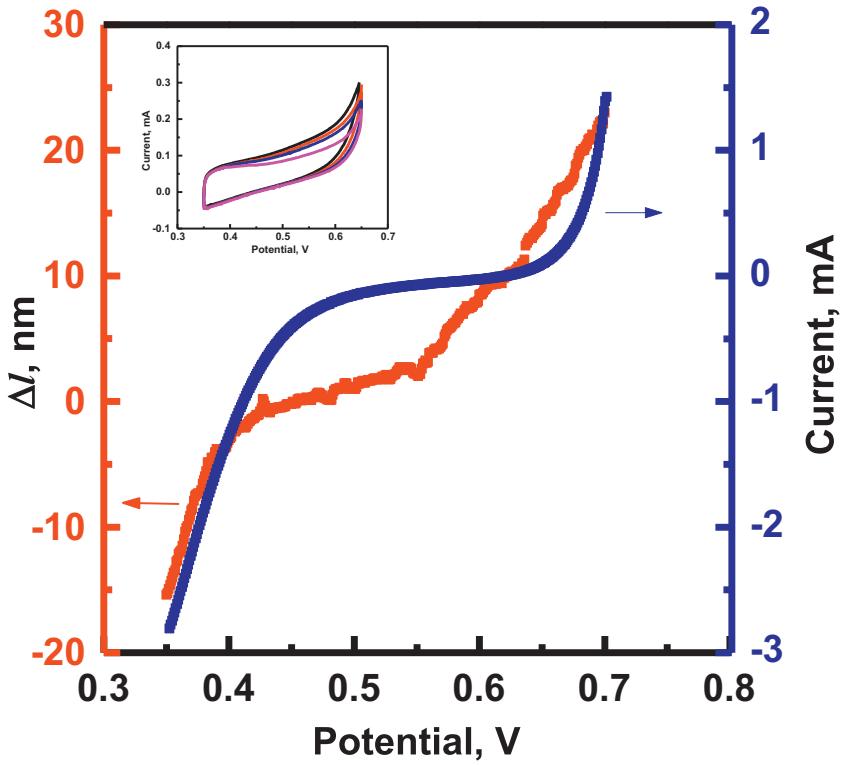

Fig. 3. Macroscopic length changes Δl measured from EC-AFM during potential scan from 0.35 V to 0.7 V in 0.5 M Na_2SO_4. The inset figure is cyclic voltammograms within the potential range 0.35–0.65 V.

For the CSAFM measurements, the tip is kept in contact with the npg surface. The surfaces of polarized npg sample are covered by surface oxide, and the oxide coverage efficiently prevents coarsening due to a reduced surface diffusivity of metal. Then metal-semiconductor-metal contacts are present between the Pt-coated tip, the oxide film and the npg substrate. In this case, the flow of electrons from the semiconductor to the metal was prevented with the positive applied voltage and a substantial electrons flow from the semiconductor to the metal was enhanced with the negative applied voltage, suggesting the n-type semiconductor behavior [29]. For the p-type semiconductor, similar arguments can be applied. Thus, when almost symmetric and asymmetric I-V curves present high resistance with positive applied voltage, the semiconductor is regarded as the n-type. Oppositely, if it has higher resistance with negative applied voltage, then the semiconductor is thought to be the p-type. Based on the I-V curves obtained in this study, the oxides on the npg surface are complex and can vary. It is well known that n- or p-type semiconductor properties are related to the sample chemical composition. Generally, Au is inert and it is difficult to form oxide, while silver is likely to form Ag_2O and AgO oxides in electrochemical dealloying. Ag_2O behaves as the p-type semiconductor, attributed to silver or cation vacancies, while AgO exhibits the n-type semiconductor properties attributed to oxygen vacancies trapped in the oxide film. These oxides densely cover the npg sample surface, suppressing the np structure coarsening. CSAFM studies point to the importance of oxide coverage influencing the corrosion kinetics. However, more experiments are needed to provide a clear explanation of the dealloying mechanism.

Fig. 3 shows the changes of reduced sample NPG-3 macroscopic length with the applied voltage from the EC-AFM measurements. The inset figure in Fig. 3 shows the CVs with the potential range of 0.35–0.65 V. These are typical CV curves and well reproducible. When a bias is applied between the surface and the probe, the probe cantilever produces the corresponding deviation. The sample macroscopic length changes are measured from the cantilever deflection. One can obtain the change of the tip bias passing through the probe. Then the macroscopic dimension changes of npg sample can be calculated according to the theoretical model. Due to the cantilever probe being sensitive to the displacement change, this method can be used to measure small macroscopic deformations. Fig. 3 shows the results of the *in-situ* EC-AFM tests in 0.5 M Na_2SO_4. The sample length change Δl in the positive scan from 0.35 V to 0.7 V is about 40 nm. The npg sample dimension expanded with the applied voltage. This is also consistent with the observations of Jin et al. [23]. The macroscopic strain amplitude is 0.003% for the 1.2 mm thick sample. Thus, *in-situ* EC-AFM measurements are accurate for quantifying these evolutions in electrochemical environment.

It was demonstrated that the initial prepared npg sample NPG-1 and polarized sample NPG-2 exhibit a small ligament size of about 15 nm, and the reduced sample NPG-3 has a larger ligament size of 30–40 nm. The oxide layer formed in the electrochemical dealloying process leads the small np structure of npg samples. The CSAFM results reveal that the Ag_2O species behave as the p-type semiconductor, while AgO exhibits n-type semiconductor properties. In conclusion, the oxide on npg surface can effectively suppress the np structure coarsening. The EC-AFM measurements show that the npg sample length change during the positive potential scan from 0.35 V to 0.7 V is 40 nm.

Acknowledgments

This work was supported by the National Natural Science Foundation of China (51801010), China Postdoctoral Science Foundation (2018M631336) and the Fundamental Research Funds for the Central Universities (FRF-TP-17-018A1).

References

[1] A. Wittstock, V. Zielasek, J. Biener, C.M. Friend, M. Baeumer, Science 327 (2010) 319.
[2] Y. Ding, M.W. Chen, J. Erlebacher, J. Am. Chem. Soc. 126 (2004) 6876.
[3] G. Pia, E. Sogne, A. Falqui, F. Delogu, Sci. Rep. 8 (2018) 15208.
[4] A. Pröschel, J. Chacko, R. Whitaker, M.A.U. Chen, E. Detsi, J. Electrochem. Soc. 4 (2019) 166.

[5] E. Detsi, M. Salverda, P.R. Onck, J.T.M. De Hosson, J. Appl. Phys. 115 (2014) 044308.
[6] X. Lang, A. Hirata, T. Fujita, M.W. Chen, Nat. Nanotechnol. 6 (2011) 232.
[7] H.J. Jin, X.L. Wang, S. Parida, K. Wang, M. Seo, J. Weissmüller, Nano Lett. 10 (2010) 187.
[8] J. Weissmüller, R.N. Viswanath, D. Kramer, P. Zimmer, R. Wurschum, H. Gleiter, Science 300 (2003) 312.
[9] E. Detsi, S. Punzhin, J. Rao, P.R. Onck, J.T.M. De Hosson, ACS Nano 6 (2012) 3734.
[10] E. Detsi, S.H. Tolbert, S. Punzhin, J.T.M. De Hosson, J. Mater. Sci. 10 (2015) 1007.
[11] C. Stenner, L.H. Shao, N. Mameka, J. Weissmüller, Adv. Funct. Mater. 26 (2016) 5174.
[12] S.O. Kucheyev, J.R. Hayes, J. Biener, T. Huser, C.E. Talley, A.V. Hamza, Appl. Phys. Lett. 89 (2006) 053102.
[13] J.F. Huang, I.W. Sun, Adv. Funct. Mater. 15 (2005) 989.
[14] M. Hieda, R. Garcia, M. Dixon, T. Daniel, D. Allara, M.H.W. Chan, Appl. Phys. Lett. 84 (2004) 628.
[15] E. Detsi, Z.G. Chen, W.P. Vellinga, P.R. Onck, J.T.M. De Hosson, J. Nanosci. Nanotechnol. 11 (2012) 4951.
[16] E. Detsi, Z.G. Chen, W.P. Vellinga, P.R. Onck, J.T.M. De Hosson, Appl. Phys. Lett. 99 (2011) 083104.
[17] Y. Yu, L. Gu, X.Y. Lang, C.B. Zhu, T. Fujita, M.W. Chen, J. Maier, Adv. Mater. 23 (2011) 2443.
[18] E. Detsi, X. Petrissans, Y. Yan, J.B. Cook, Z.L. Deng, Y.L. Liang, B. Dunn, S.H. Tolbert, Phys. Rev. Materials 2 (2018) 055404.
[19] H. Gao, J.Z. Niu, C. Zhang, Z.Q. Peng, Z.H. Zhang, ACS Nano 12 (2018) 3568.
[20] S. Van Petegem, S. Brandstetter, R. Maass, A.M. Hodge, B.S. El-Dasher, J. Biener, B. Schmitt, C. Borca, H. Van Swygenhoven, Nano Lett. 9 (2009) 1158–1163.
[21] J. Erlebacher, M.J. Aziz, A. Karma, N. Dimitrov, K. Sieradzki, Nature 410 (2001).
[22] J. Erlebacher, J. Electrochem. Soc. 151 (2004) C614–C626.
[23] H.J. Jin, S. Parida, D. Kramer, J. Weissemüller, Surf. Sci. 602 (2008) 3588–3594.
[24] F. Kertis, J. Snyder, L. Govada, S. Khurshid, N. Chayen, J. Erlebacher, JOM 62 (2010) 50–56.
[25] Y. Ding, Y.J. Kim, J. Erlebacher, Adv. Mater. 16 (2004) 1897–1900.
[26] J. Snyder, P. Asanithi, A.B. Dalton, J. Erlebacher, Adv. Mater. 20 (2008) 4883.
[27] E. Detsi, M. Van de Schootburgge, S. Punzhin, P.R. Onck, J.T.M. De Hosson, Scr. Mater. 64 (2011) 319.
[28] T. Souier, F. Martin, C. Bataillon, J. Cousty, Appl. Surf. Sci. 256 (2010) 2434.
[29] M.C. Lin, G. Wang, L.Q. Guo, L.J. Qiao, Alex A. Volinsky, Appl. Phys. Lett. 103 (2013) 143118.